Persistent confined migration confers permanent nuclear and functional changes in migrating cells.

Ana de Lope-Planelles[1], Raquel González-Novo[1], Elena Madrazo[1], Héctor Zamora-Carreras[2], Verónica Torrano[3], Horacio López-Menéndez[4,5], Pedro Roda-Navarro[2], Francisco Monroy[4,5], Javier Redondo-Muñoz[1*].

[1]Department of Molecular Medicine, Centro de Investigaciones Biológicas Margarita Salas (CIB Margarita Salas-CSIC), Madrid, Spain. [2]Department of Immunology, School of Medicine, University Complutense de Madrid and 12 de Octubre Health Research Institute (Imas12) Madrid, Spain. [3]Department of Biochemistry and Molecular Biology, University of the Basque Country, Leioa, Spain. [4]Department of Physical Chemistry, Complutense University, Madrid, Spain. [5]Translational Biophysics, Hospital Doce de Octubre Health Research Institute (imas12), Madrid, Spain.

Short title: Confined migration and permanent nuclear changes.

Keywords: Cell migration, nuclear deformability, mechanobiology, lamin, DNA damage.

***Corresponding author**: Javier Redondo-Muñoz. javier.redondo@cib.csic.es.

Highlights

- Persistent confined migration promotes permanent mophological changes.
- Lamin B1 is redistribution in the nucleus of migratory altered cells.
- Migratory-altered cells exhibit transcriptional and functional changes related to cell migration and survival.
- Actin polymerization controls nuclear changes induced by cell migration.

Abstract

Nuclear deformability plays a critical role in cell migration. During this process, the remodeling of internal components of the nucleus has a direct impact on DNA damage and cell behavior; however, how persistent migration promotes nuclear changes leading to phenotypical and functional consequences remains poorly understood. Here, we described that the persistent migration through physical barriers was sufficient to promote permanent modifications in migratory-altered cells. We found that lamin B1 altered its localization, concomitant with morphological and transcriptional changes. Migratory-altered cells showed alterations in cellular functions such as DNA repair and cell migration. We applied biochemical and biophysical approaches to identify that confined conditions altered the biomechanical response of the nucleus. Mechanistically, we determined that actin dynamics controlled the redistribution of lamin, and the basal levels of DNA damage in migratory-altered cells. Our observations reveal a novel role for confined cell conditions in consistent nuclear and genomic alterations that might handle the genetic instability and cellular heterogeneity in aging diseases and cancer.

38 **Introduction**

39 Cell migration is a fundamental process involved in physiological and pathological conditions
40 such as development, immune response, inflammation, and cancer invasion [1, 2]. Migrating
41 cells have to cross through different tissue environments, including the extracellular matrix
42 and endothelial barriers, which provide multiple biochemical and mechanobiological signals
43 for an active and effective cell migration [3, 4]. Nuclear deformability has been defined as a
44 major limiting factor for cell migration across physical barriers [5]. The nucleus is a highly
45 dynamic organelle composed of the nuclear envelope, the lamina network, and the chromatin
46 structure [6-8]. The cytoskeleton exerts and transmits mechanical forces and external stimuli
47 into the nucleus [9, 10]; and previous studies have demonstrated that nuclear deformation
48 induced by mechanical stress regulates chromatin changes, DNA damage response, and cell
49 stemness [11-15]. Likely, several human pathologies are associated with defects in the
50 response of the nucleus to mechanical stimuli, including progeria, cardiomyopathies, and
51 cancer [16, 17]. However, how much persistent migration might control more stable nuclear
52 changes remains poorly understood.

53 On this basis, we compare two cell migration settings, one-round migration (ORM) cells, and
54 migratory-altered (MA) cells, which might promote nuclear changes while regulating the
55 functional and mechanical responses of the cell in two differential mechanobiological
56 scenarios. We have found that cell migration triggers a change in the distribution of lamin B1
57 and the accumulation of DNA damage markers. To elucidate the functional consequences of
58 nuclear changes induced by persistent cell migration, we explored how moving cells might
59 alter their gene expression signature and other cellular functions. We demonstrated that the
60 mechanical stress during cell migration generates permanent changes in the transcriptional
61 profile of migratory-altered cells. Furthermore, strong nuclear deformability under persistent
62 cell migration alters a range of mechanical and functional responses, including cell migration,

63 and DNA damage repair. Noticeably, latrunculin treatment causes lamin B1 localization at the
64 nuclear periphery and rescues the basal phenotype and morphology of the nucleus and
65 chromatin compaction, suggesting that actin polymerization is critical for some of these
66 processes. Overall, our experimental findings offer insight into how nuclear deformability
67 induced by cell migration contributes to genomic alterations, which could lead to functional
68 changes, such as tumor progression and heterogeneity of cancer cells.
69
70 **Results**
71 **Mechanical constriction promotes morphological changes in the nucleus of migrating**
72 **cells.**
73 We first determined how confined migration alters the nuclear morphology of migrating cells.
74 We seeded leukemia cells on rigid filter membranes and allowed their migration (one-round
75 migration, ORM) through the pores for 24 h. Then, we collected these cells and compared
76 them with their non-migrating counterparts to further characterize how cell migration through
77 physical barriers might influence the nucleus of leukemia cells. First, we observed that ORM
78 cells increased their nuclei in comparison to non-migrating cells (Figures 1A, 1B, S1A and
79 S1B). It has been shown that changes in the size of isolated nuclei can be determined by flow
80 cytometry [18], and we verified that isolated nuclei from ORM cells showed bigger size than
81 nuclei from non-migrating cells (Figure S1C). To understand the long-term consequences of
82 persistent cell migration, and whether a consistent migratory stimulus might induce similar
83 changes to ORM cells, we generated stable migratory-altered (MA) cells, by allowing cells to
84 migrate three–rounds across rigid filter membranes and then culturing them in the absence of
85 further mechanical stimuli (Figure 1C). We visualized the nucleus of MA cells and confirmed
86 that persistent cell migration also induced an increment in the size of the nucleus (Figures 1D,
87 1E, S1C, and S1D). These results were in line with our observations above, which showed

88 that ORM cells presented bigger nuclei compared to control cells. Together, these data
89 indicate that cell squeezing during migration induces changes in the nuclear size of moving
90 cells. Having observed differences in the size of the nuclei, we next focused in the nuclear
91 morphology of MA cells. Electron microscopy images revealed a remarkable aberrant
92 morphology of the nucleus of MA cells compared to those from control cells (Figures 1F, and
93 S1E); although we did not observe differences in the nuclear morphology of ORM cells
94 (Figures S1F, and S1G). This suggests that increasing nuclear size is a common effect of
95 confined migration, whilst altering nuclear morphology might only be characteristic in the
96 context of persistent migration.

97 **Persistent migration alters permanently the lamin B1 distribution within the nucleus.**

98 Since nuclear lamina controls the mechanical properties and behavior of the nucleus [19], we
99 next sought to elucidate whether confined migration promoted alterations in the lamina
100 network and found that constricted migration altered the distribution of lamin B1 in ORM
101 cells (Figures 2A, and S2A). While non-migrating cells showed two characteristic peaks for
102 lamin B1 signal in the transversal section of the nucleus (corresponding to the nuclear
103 periphery), ORM cells presented an aberrant distribution of lamin B1 (Figures 2B, S2B, and
104 Movies S1, S2). Temporal changes in internal components might critically regulate the
105 morphology of the nucleus in moving cells; therefore, the nuclear volume and lamin B1
106 redistribution observed would be recovered in ORM cells once the migratory effect
107 disappears. We demonstrated that ORM cells cultured in suspension for an additional 24
108 hours reduced their nuclear size to levels comparable to those from non-migrating cells
109 (Figures 2C, 2D, S2C, and S2D). Furthermore, these cells also recovered the normal
110 localization of lamin B1 at the nuclear periphery (Figures 2E, and S2E). To investigate the
111 effect of persistent migration on the nuclear changes of MA cells, we determined their lamin
112 B1 distribution and found that MA cells showed an aberrant distribution of lamin B1 (Figures

113 2F, 2G, S2F, S2G, and Movies S3, S4). These findings led us to conclude that persistent
114 migration is a critical factor to induce permanent alterations in moving cells, whilst transient
115 migration shows only a temporary effect on the nucleus of migrating cells. Altogether, these
116 results indicate that moving cells derived both from transient and persistent migration
117 underwent lamin B1 redistribution, which can affect multiple cellular functions.

118 **Persistent migration induces enduring changes in the transcriptional profile of**
119 **migrating cells.**

120 It has been previously described that nuclear shape regulates the transcriptional activity of
121 cells [20, 21]. As MA cells showed a different and sustained phenotype compared to control
122 cells, we hypothesized that persistent cell migration might produce enduring changes in the
123 transcriptional landscape of MA cells. We evaluated the expression levels of transcripts of
124 control or MA cells and found a significant differential expression of 1.8-fold change in 639
125 genes (285 up- and 354 down-regulated) in MA cells compared with control cells (Figures
126 3A, S3A, and Table S1). We next extended our observation to KEGG (Kyoto Encyclopedia of
127 Genes and Genomes) and GO (Gene Ontology) enrichment analyses, which revealed that
128 most of the altered genes were connected to cell division, survival, DNA damage checkpoints
129 and protein modification (Figure S3B). To confirm changes in gene expression identified by
130 microarray analysis, we measured the relative mRNA levels of two genes related to leukemia
131 (*EZH2* and *JAK2*), as well as the expression levels of 5 randomly selected proteins (Figures
132 3C, S3C, and S3D). Once validated these observations, our pathway analysis demonstrated
133 that upregulated genes of MA cells encode proteins related to G2/M progression, mitotic
134 spindle, and chromosome segregation (Figure 3B, and Table S2). Previous reports showed that
135 confined conditions regulate cell proliferation and cell cycle progression [22, 23]; however,
136 we observed no differences in the proliferative properties of MA cells compared to control
137 cells (Figures 3D, 3E, S3E, and S3F). We validated that the cell cycle progression was not

138 altered in MA cells (Figures 3F, and S3G), suggesting that cell proliferation might be affected
139 by other external stimuli, rather than just potential transcriptional changes. Overall, our results
140 indicate that persistent cell migration might induce changes in the transcriptional profile of
141 moving cells.

142 **Migrating cells show altered basal levels of DNA damage markers and resistance to**
143 **apoptosis.**

144 In addition to controlling the cell cycle progression, cell migration is also known to favor
145 DNA damage upon extreme nuclear deformability [24]. We investigated whether cell
146 migration might increase the constitutive levels of γH2AX (a well-known DNA damage
147 marker) and found that most of the non-migrating cells showed low levels of γH2AX (<2 foci
148 per nucleus), in contrast to fresh ORM cells (Figures 4A). Likely, the percentage of positive
149 MA cells for γH2AX was higher than control cells (Figures 4B, and 4C), indicating that cell
150 migration increases the basal levels of DNA damage in moving cells. This suggests that cells
151 undergoing transient and persistent migration increase their basal levels of DNA damage,
152 which would presumably have an impact on how leukemia cells respond to therapy. Our
153 pathway analysis showed that MA cells might downregulate genes involved in endoplasmic
154 reticulum stress and unfolded protein response (Figures 4D and Table S2), which might be
155 relevant for drug resistance in cancer (25). To gain insight into how persistent migration
156 might affect cell viability, we treated control and MA cells with methotrexate, a DNA
157 biosynthesis inhibitor used in clinics against multiple human pathologies [26]. Interestingly,
158 we found that MA cells showed higher resistance to apoptosis than control cells (Fig. 4E, 4F).
159 While this is a simple model to induce apoptosis, we could speculate that MA cells would
160 turn less sensitive to some conventional therapies compared to control cells. Overall, these
161 observations indicate that persistent migration would facilitate the resistance to apoptosis and
162 the adaptation to conventional therapies of invasive moving cells.

163 **Migrating cells show different biomechanical responses of the nucleus and altered cell**
164 **invasiveness.**

165 Lamins and chromatin contribute to the mechanical properties and size of the nucleus [27],
166 and we hypothesized that confined migration might control not only the nuclear morphology
167 but also have a direct impact on the mechanical behavior of the nucleus. We assayed an
168 external mechanical pressure technology to exert forces onto isolated nuclei from control and
169 MA cells [28], and observed that the nuclei of MA cells increased 2.5-fold under external
170 pressure, whilst control cells showed only 1.77-fold (Figures 5A, 5B, S4A, and S4B). This
171 indicates that MA cells showed a higher nuclear deformation capacity compared to control
172 cells. Then, we trapped isolated nuclei from control and MA cells and analyzed them with
173 optical tweezers. Unexpectedly, isolated nuclei from MA cells showed no differences in their
174 stiffness and water diffusivity compared to control cells (Figures 5C, and 5D). It is possible
175 that the response generated by optical tweezers represented a different mechanical behavior
176 than the whole compression of the nucleus. To further characterize the mechanical behavior
177 of the nucleus, we addressed its response under osmotic stress. The balance of cations
178 regulates the osmotic pressure and the chromatin compaction in the nucleus [29]. We
179 observed that isolated nuclei from MA cells responded better to the addition of cations (42%
180 of shrinking compared to 10% of nuclei from control cells), whilst the addition of EDTA
181 promoted higher swelling in isolated nuclei from control cells rather than from MA cells
182 (60% and 30% of increment in the nuclear area, respectively; Figures 5E, and 5F). To
183 compare these findings with transitory changes induced by cell migration, we isolated nuclei
184 from ORM cells and observed an increment in their nuclear deformability area upon
185 compression by external forces (Figures S4C, and S4D). Furthermore, isolated nuclei from
186 ORM cells showed higher nuclear stiffness and diminished water diffusivity compared to
187 non-migrating cells (Figures S4E, and S4F).

188 As nuclear deformability is a critical stage for cell invasion [12], we assayed how permanent
189 changes induced by constrained migration might affect this cellular function. First, we
190 characterized *in vitro* that MA cells showed a higher chemotactic response compared to
191 control cells (Figure S5A). Interestingly, MA cells showed a similar capacity to penetrate into
192 a 3D collagen matrix as control cells (Figures 5G, and S5B). To determine the migratory
193 capacity of MA cells and their ability to infiltrate into the bone marrow and spleen of
194 immunodeficient mice [30], we injected an equal number of control and MA cells labeled
195 with vital dyes into the tail vein of recipient mice and found a reduction of MA cells reaching
196 these tissues related to harboring metastatic leukemia cells (Figures 5H, and S5C). These
197 results indicate that constrained migration alters the mechanical behavior of the nucleus,
198 which might have functional implications on the capacity of MA cells to infiltrate tissues.

199 **Actin homeostasis controls lamin B1 redistribution and the nuclear changes observed in**
200 **migrating cells.**

201 Actin polymerization regulates the nuclear morphology and chromatin remodeling upon
202 cellular constrictions [31, 32]. As we found that nuclear lamin B1 redistributed in MA cells,
203 we used specific drugs to depolymerize or stabilize actin filaments. We observed that
204 latrunculin (an inhibitor against actin polymerization) treatment was sufficient to rescue the
205 localization of lamin B1 at the nuclear periphery in MA cells (Figures 6A, 6B, S6A, and
206 S6B). Likely, MA cells treated with latrunculin showed a reduction in the nuclear area, whilst
207 the pharmacological stabilization of polymerized actin with jasplakinolide did not promote
208 any effect (Figure 6C). In addition to actin polymerization, several kinases trigger lamin B1
209 redistribution, such as Cdk1 (cyclin-dependent kinase 1) and protein kinase C (PKC) [33]. To
210 determine whether these kinases might affect the phenotype observed in MA cells, we
211 incubated these cells with specific inhibitors and observed that none of them rescued the
212 normal lamin B1 redistribution (Figure S6C). Moreover, we did not see any reduction in the

213 nuclear area of MA cells upon these treatments, and even the Cdk1 inhibitor (roscovitine)
214 seemed to increase it (Figure S6D). Given that actomyosin controls the nuclear size and
215 chromatin compaction [34, 35], we next investigated whether actin polymerization might also
216 regulate the global the chromatin conformation in MA cells. We treated control and MA cells
217 with DNAse I and found that MA cells were less sensitive to DNA digestion, suggesting a
218 different global chromatin compaction. Furthermore, latrunculin treatment reverted this
219 change in MA cells, which showed a DNA digestion profile more similar to control cells
220 (Figures 6D, 6E, S6E and S6F). To further confirm this point, we performed *in situ* DNA
221 digestion and observed that control cells were more sensitive to DNA digestion (visualized as
222 a reduction in the nuclear area by DNAse activity) than MA cells (Figure S6G). Finally,
223 several reports show that actin cytoskeleton is required during DNA damage response [36,
224 37]. We investigated the levels of γH2AX in MA cells treated with latrunculin and
225 jasplakinolide, and found that γH2AX were reduced in MA cells treated with latrunculin,
226 whereas jasplakinolide treatment exhibited a more similar phenotype to untreated MA cells
227 (Figures 6F, and 6G). Taken together, our results indicate that actin polymerization regulates
228 several of the permanent nuclear changes induced by persistent cell migration in MA cells.
229

230 **Discussion**

231 In this work, we pointed out a connection between cell migration and permanent changes in
232 the nucleus that lead to functional consequences in cell biology. The nucleus is a
233 mechanosensory organelle that has to alter its mechanical and morphological characteristics
234 for multiple cellular functions, including migration, development, and cancer progression [38,
235 39]. To undergo migration, cells have to sense their physiological environment to control their
236 integrity and functions [40-42]. This is particularly important as extracellular migratory and
237 mechanical signals regulate the adaptability of cells, their stemness, differentiation, genomic

238 instability. Therefore, nuclear changes in response to cell migration might represent a major
239 medical issue in many human diseases, including cancer infiltration [43-45].
240 Despite previous evidence showing that cell migration through confined spaces promotes
241 nuclear ruptures, protein redistribution, and DNA damage nuclear alterations [46-48], their
242 long-term consequences remain unclear. The impact of mechanobiology in stem cell
243 reprogramming and cell rejuvenation has been previously described [49, 50], suggesting that
244 cell confinement might influence memory effects and the fate transition of migratory cells.
245 Our persistent cell migration approach shows that cells adapted to several rounds of cell
246 migration by altering their nuclei in a permanent manner. This is particularly important as
247 MA cells kept in culture showed a different phenotype and nuclear changes (including nuclear
248 morphology and lamin B1 redistribution), which remain even without further cellular
249 constriction. This transition highlights how cells might respond depending on the migratory
250 stimulus and whether this is occasional or repeated. In addition, our data support that
251 persistent migration controls altered transcription and phenotypical changes that agree with
252 previous studies showing how biophysical stimuli control cell fate and differentiation [51,
253 52]. Mechanical stress between the cell and its environment is known to regulate cell cycle
254 progression and genomic instability that leads hyperploidy [53, 54]. Although we did not see
255 significant changes in cell proliferation, we cannot discard that under physiological conditions
256 or external stimuli these changes might have potential implications in promoting cell state
257 alterations and genomic instability and heterogeneity in cancer cells.
258 Due to the reported role of the nucleus as a mechanosensor [55], we analyzed the mechanical
259 features of cells upon persistent and transient migration. To overcome the complexity of the
260 mechanical analysis of isolated nuclei, we designed an experimental rationale based on
261 nuclear swelling, nuclear compression, and indentation by optical tweezers. Previous works
262 show nuclear swelling and compression as good experimental approaches to define the

263 mechanical response of the nucleus [56-58]. In our experiments, the nucleus exhibits a two-
264 regime response, depending on occasional or persistent cell migration. Considering the fact
265 that migrating cells suffer different degree of mechanical stress on their nuclei; after a sole
266 migration event, ORM cells might show some heterogeneity in their nuclear mechanical
267 properties. On the other hand, MA cells could have developed a sort of homogeneous
268 accommodation of the nuclear internal architecture due to the repeated application of a
269 mechanical stress during cell migration, showing similar stiffness and poroelastic diffusivity.
270 Permanent changes during the time of migratory cells may act in parallel or independently of
271 other cellular functions. Interestingly, we described defective colonization of MA cells into
272 different organs. This suggests that other molecular pathways could also be regulating the
273 migration strategy used by MA cells, which might become less invasive than control leukemia
274 cells. A plausible explanation might be a migratory exhaustion of MA cells, which would
275 transit from a more effective movement into a more static condition. This versatility would be
276 particularly important in several pathologies, including cancer, where invasive cells might
277 switch into a heterogeneous population priming other cellular functions, such as cell cycle and
278 resistance to apoptosis. Recent studies with normal and tumor cells have described the
279 localization and upregulation of several markers of DNA damage in migratory cells under
280 high nuclear deformation [59]. So far, nuclear lamins and deformability seemed to be
281 involved in cell growth, DNA damage response, and cellular stress [16, 60]. From a clinical
282 perspective, we pretended to confirm whether MA cells might show a therapeutic advantage
283 in comparison to control leukemia cells. MA cells showed high basal levels of γH2AX but
284 resisted apoptosis better than control cells. This chemoresistance to antimetabolites might be
285 due to differences in cell proliferation or the metabolic activity of tumor cells [61].
286 Interestingly, we did not find changes in the proliferation of MA cells, which also show a
287 downregulation of genes related to unfolded protein response and endoplasmic reticulum

288 stress, fundamental in chemoresistance [62]. A plausible explanation is that under specific
289 circumstances aberrant nuclear changes and high basal levels of γH2AX would be protective
290 for MA cells against specific conventional therapies. This agrees with the idea that the steady
291 state of γH2AX is critical for cell cycle regulation and the maintenance of genomic integrity
292 [63, 64]. Our findings suggest that the potential adaptation of MA cells might have a dual
293 effect on reducing their ability to reach other tissues, and on promoting other functions, such
294 as cell survival and proliferation.
295 The cell skeleton, including actin polymerization and its associated proteins, is critical in many
296 nuclear events, including chromatin compaction, and gene transcription. [65-67]. One exciting
297 implication of our results is that actin depolymerization seemed to recapitulate the DNAse
298 sensitivity of the chromatin in MA cells, in parallel to their lamin B1 redistribution at the
299 nuclear periphery. Our observation also aligns with other results where actin homeostasis
300 drugs alter the chromatin structure [68]. In fact, it has been reported that the actin
301 cytoskeleton is critical for nuclear integrity and DNA repair in constricted migration [69];
302 and, in agreement with this, we observed that actin perturbation also reduced the levels of
303 γH2AX in MA cells. Together, our findings highlight new knowledge about how cell
304 migration underlies permanent nuclear changes that might lead to morphological,
305 transcriptional, and functional changes in moving cells.
306 In conclusion, our findings highlight how migratory cells respond in structurally regulated
307 ways to mechanical compression both in the short- and long-terms. We revealed a novel
308 effect of persistent cell migration in morphological and transcriptional changes, which
309 provides novel insights into alterations in the nucleus and functions of the cell. Furthermore,
310 we have described how actin polymerization regulates the nuclear morphology and lamin B1
311 redistribution, supporting the relevance of molecular connections between the cell skeleton
312 and nuclear changes induced by the cell environment interplay. Finally, we would like to

313 propound the notion that cell migration underlies permanent nuclear changes that might lead
314 to cell fate transition, genomic instability, and cellular heterogeneity with broad implications
315 for development, aging, cancer, and mechanobiological processes.
316
317 **Materials and methods**
318 **Cell lines and culture.** The human Jurkat (CVCL_0367) and CCRF-CEM (RRID:
319 CVCL_0207) cell lines were from ATCC, American Type Culture Collection. Both cell lines
320 were monthly tested for mycoplasm contamination and maintained in culture in RPMI 1640
321 medium with L-glutamine and 125 μM HEPES (Sigma Aldrich, St. Louis, MO, USA) and
322 10% fetal bovine serum (Sigma-Aldrich) and maintained in 5% CO_2 and 37ºC.
323 One-round migration (ORM) cells were collected from the bottom chamber of Transwell
324 inserts (Corning Costar, 6.5 mm diameter, 3 μm pore size) after 24h. For recovery assays,
325 collected ORM cells were used to performed experiments (fresh condition); or kept in culture
326 conditions for an additional 24h and then used to performed experiments (after 24h
327 condition). Migratory-altered (MA) cells were generated as follows: Jurkat or CCRF-CEM
328 cells were allowed to migrate in transwells for 24h; then, migrated cells were collected from
329 the bottom chamber, counted and added again to the upper chamber of new inserts, under the
330 same conditions. The same process was repeated 3 times. Finally, migrated cells from the
331 bottom chamber were collected, expanded and kept in culture conditions as MA cells.
332 **Immunofluorescence.** Cells were cultured in suspension, treated or not with specific
333 inhibitors, for 1 hour at 37ºC. Cells were seeded onto poly-L-lysine-coated glass slides for 30
334 min. Then, cells were fixed with 4% formaldehyde (15 min) and permeabilized with 0.5% Tx-
335 100 in PBS (5 min). Samples were blocked in 10% fetal bovine serum with 0.1% Tx-100 in
336 PBS, incubated with appropriated primary antibodies for 1h at RT, followed by several PBS
337 washes and 1h at RT incubation with secondary antibodies. Samples were stained with DAPI

338 1 μg/mL for 10 min at RT, washed with PBS and H_2O, and mounted. Images were acquired
339 on an inverted DMi8 microscope (Leica) using an ACS-APO 63x NA 1.30 glycerol
340 immersion objective. Quantification and analysis of images were determined using ImageJ.
341 **Electron microscopy.** Cells were fixed for 1h in 3% glutaraldehyde in PBS and then washed
342 twice with PBS. Samples were post-fixed in 1% osmium tetroxide and 0.8% potassium
343 ferricyanide for 1h at 4ºC and washed with PBS prior to dehydration with an increasing
344 gradient of ethanol (30%, 50%, 70%, 80%, 90% and 100%) of 10 min per step. Samples were
345 embedded in LX112 resin and were polymerized for 48h at 60ºC. 60-80 nm sections were
346 placed in copper grids of 75 mesh and stained with 5% uranyl acetate for 30 min and lead
347 citrate for 4 min. Samples were viewed in a JEOL 1230 TEM and images were taken with a
348 CMOS TVIPS 16 mp camera.
349 **Nuclear confinement**. Cell nuclei were isolated by incubating cells in buffer A (10 μM
350 HEPES, 10 μM KCl, 1.5 μM $MgCl_2$, 0.34 M sucrose, 10% (v/v) glycerol, 1 μM DTT and
351 Roche protease inhibitor cocktail) for 5 min at 4ºC and centrifuged for 5 min at 4°C at 3,500
352 rpm. Nuclei were resuspended in TKMC buffer (50 μM Tris pH 7.5, 25 μM KCl, 3 μM
353 $MgCl_2$, 3 μM $CaCl_2$), dyed with DAPI 1 μg/mL and sedimented onto poly-L-lysine coated
354 plate for cell confinement analysis (4D cell). In this case, a glass slide with micropillars of 3
355 μm height was stuck on the silicone macropillar attached to the lid of the confiner. When the
356 lid was closed, the pillars pushed the confining slides onto the culture substrate and confined
357 the nuclei to 3 μm. Images of at least 20 nuclei were taken with a 63× objective before and
358 after the confinement by an inverted confocal microscope.
359 **Flow cytometry.** Isolated nuclei were resuspended in TKMC buffer and nuclear size was
360 measured with a CytoFlex (Beckman Coulter). To analyze protein levels, cells were blocked
361 with human IgG (1:1000; 30 min), incubated with specific primary antibodies of interest (1:1
362 to IgG), washed twice with PBS, followed by appropriated fluorochrome-conjugated

363 secondary antibody for 30 min. Flow cytometry was performed with a FacSort. All data were
364 analyzed using the Flow Jo software (Flow Jo LLC, Ashland, OR, USA).
365 **Optical tweezers**. Isolated cell nuclei resuspended in TKM buffer were mixed with
366 polystyrene beads with a mean particle size of 3.0 μm (Sigma-Aldrich) at final concentrations
367 of 10^7 nuclei/ml and 0.005% (w/v), respectively. The optical tweezers device (SensoCell,
368 Impetux Optics S.L., Spain) is equipped with an ultra-stable single-frequency laser source (5
369 W, λ = 1064 nm) guided by acousto-optic deflectors and includes a direct force measurement
370 platform capable of detecting the light scattered from the optical traps. The OT device is
371 mounted on an inverted microscope (Eclipse Ti, Nikon, Japan) and a water immersion
372 objective (Plan Apo VC 60XA/1.20 WI, Nikon) employed to focus the laser on the sample. A
373 short-pass dichroic mirror transmits the bright-field illumination and reflects the IR trapping
374 beam, and a short-pass filter was used to avoid IR laser radiation leaking. Sample bright-field
375 imaging was captured by a CMOS camera (DCC1545M-GL, ThorLabs, USA) and the optical
376 traps were operated with LightAce software (Impetux Optics S.L.). For each indentation
377 experiment, a volume of 40 μL of the sample was placed in a custom-made glass chamber.
378 This chamber was mounted on the microscope and measurements were performed at 25 ºC.
379 Only average-sized, round, symmetric nuclei with no alterations or major perturbations of
380 their integrity were selected to perform the indentation routine. Indented nuclei got attached to
381 the bottom surface of the glass chamber by unspecific interactions, and indenter beads were
382 placed next to the nuclear envelope at axial positions and approximately 2 μm above the
383 bottom surface of the chamber. Indenter beads had a nominal diameter of 3 μm, but the exact
384 diameter of each bead used for indentation was measured by image analysis using the Fiji
385 software. The indentation process consisted on pushing the nucleus laterally by generating an
386 oscillation of the indenting bead. The fixed parameters of the oscillation are the shape
387 (squared), frequency (0.5 Hz, which is enough to permit a complete relaxation between

388 consecutive cycles), and offset (100%). The amplitude was variable, and the routine was set
389 to sweep the 0.6-1.6 μm range with steps of 0.05 or 0.10 μm. Data were acquired during 45 s
390 for each amplitude step. For each indentation experiment, the elasticity constant of the trap
391 was calculated by using a particle scan routine included in the LightAce software. We wrote a
392 specific Matlab (MathWorks, USA) script to analyze the data from the files obtained by the
393 custom-made Labview indentation routine. This script is able to isolate each force-time curve
394 for every indentation cycle and to calculate the stiffness from the indentation force values and
395 the water diffusivity from the poroelastic relaxation times.

396 **Statistics.** Statistical analysis and comparisons were made with GraphPad Prism6. The
397 numerical data are presented as mean ± SD. Differences between means were tested by
398 Student's t test for two groups comparison. Where 3 or more groups were analyzed, one-way
399 ANOVA was performed. P-values are indicated by asterisks ((*) $P < 0.05$; (**) $P < 0.01$;
400 (***) $P < 0.001$).

401

402 **Declarations**

403 **Ethics approval and consent to participate:** AAll experiments involving animals were
404 approved by the OEBA (Organ for Evaluating Animal Wellbeing) at CIB Margarita Salas and
405 Madrid Regional Department of Environment, with reference PROEX 228.4/21; and carried
406 out in strict accordance with the institution guidelines and the European and Spanish
407 legislations for laboratory animal care.

408 **Consent for publication:** All authors consent the manuscript for publication.

409 **Availability of data and materials:** The accession numbers for the transcriptional
410 microarray analyses is GSE214365. All relevant data are available from the corresponding
411 author upon reasonable request.

412 **Competing interests:** Authors declare no competing interests.

Funding: This research was supported by a FPI Scholarship 2018 (Ministerio de Ciencia e Innovación/MICINN, Agencia Estatal de Investigación/AEI y Fondo Europeo de Desarrollo Regional/FEDER) to R.G.N.; grants from the Ministerio de Ciencia e Innovación (MICINN) Agencia Estatal de Investigación (AEI) (RTI2018-097267-B-I00), Asociación Española Contra el Cáncer (LAB AECC, LABAE211656TORR) and Beca FERO (BFERO2021.01) to V.T.; Comunidad de Madrid (Y2018/BIO-5207) and from the Ministerio de Ciencia e Innovación (MICINN) Agencia Estatal de Investigación (AEI) (PID2020-115444GB-I00) to P.R.N; grants from the Ministerio de Ciencia e Innovación (MICINN) Agencia Estatal de Investigación (AEI) (PID2019-108391RB-100), and Comunidad de Madrid (Y2018/BIO-5207, S2018/NMT-4389 and REACT-EU program PR38-21-28 ANTICIPA-CM) to F.M.; and grants from 2020 Leonardo Grant for Researchers and Cultural Creators (BBVA Foundation), Ayuda de contratación de ayudante de investigación PEJ-2020-AI/BMD-19152 (Comunidad de Madrid), Comunidad de Madrid (Y2018/BIO-5207) and the Ministerio de Ciencia e Innovación (MICINN) Agencia Estatal de Investigación (AEI) (PID2020-118525RB-I00) to J.R.M.

Authors' contributions: A.dL.P., R.G.N., E.M., conducted experiments. H.Z.C., conducted experiments and contributed to data interpretation and discussion. V.T. contributed to data interpretation. H.L.M. conducted experiments and contributed to data interpretation. F.M., P.R.N., supervised the experiments, contributed to data interpretation and provided financing. J.R.M designed and supervised the experiments, contributed to data interpretation, wrote the paper, and provided financing.

Acknowledgements: The authors thank the Microscopy Unit of Instituto de Investigación Biosanitaria Gregorio Marañón (IiSGM) for assistance with confocal analyses. The authors are also grateful to the EM and Animal Facilities of platforms of the CIB Margarita Salas for

their assistance and support with the EM and *in vivo* experiments. The UCM-Genomic CAI Unit for their assistance with microarray experiments.

Supplementary materials include supporting material and methods, figures, tables and movies.

References

1. te Boekhorst, V., Preziosi, P., and Friedl, P. (2016). Plasticity of cell migration in vivo and in silico. Annu. Rev. Cell Dev. Biol. 32, 491-526. doi: 10.1146/annurev-cellbio-111315-125201.

2. Ridle,y A.J., Schwartz, M.A., Burridge, K., Firtel, R.A., Ginsberg, M.H., Borisy, G., Parsons, J.T., and Horwitz, A.R. (2003). Cell migration: integrating signals from front to back. Science 302, 1704-1709. doi: 10.1126/science.1092053.

3. Paul, C.D., Shea, D.J., Mahoney, M.R., Chai, A., Laney, V., Hung, W.C., and Konstantopoulos, K. (2016). Interplay of the physical microenvironment, contact guidance and intracellular signaling in cell decision making. FASEB J. 30, 2161-2170. doi: 10.1096/fj.201500199R.

4. Vining, K.H., and Mooney, D.J. (2017). Mechanical forces direct stem cell behaviour in development and regeneration. Nat. Rev. Mol. Cell Bio. 18, 728-742. doi: 10.1038/nrm.2017.108.

5. Kirby, T.J., and Lammerding, J. (2018). Emerging views of the nucleus as a cellular mechanosensor. Nat. Cell Biol. 20, 373-381. doi: 10.1038/s41556-018-0038-y.

6. Burke, B., Stewart, C.L. (2014). Functional architecture of the cell's nucleus in development, aging, and disease. Curr. Top Dev. Biol. 109, 1-52. doi: 10.1016/B978-0-12-397920-9.00006-8.

461 7. Gruenbaum, Y., and Foisner, R. (2015). Lamins: nuclear intermediate filament
462 proteins with fundamental functions in nuclear mechanics and genome regulation. Annu. Rev.
463 Biochem. 84, 131-164. doi: 10.1146/annurev-biochem-060614-034115.
464 8. Hübnet, M.R., and Spector, D.L. (2010). Chromatin dynamics. Annu. Rev. Biophys.
465 39, 471-489. doi: 10.1146/annurev.biophys.093008.131348.
466 9. Callan-Jones, A.. and Voituriez, R. (2016). Actin flows in cell migration: from
467 locomotion and polarity to trajectories. Curr. Opin. Cell Biol. 38, 12-17. doi:
468 10.1016/j.ceb.2016.01.003.
469 10. Gupta, M., Sarangi, B.R., Deschamps, J., Nematbakhsh, Y., Callan-Jones, A.,
470 Margadant, F., Mège, R.M., Lim, C.T., Voituriez, R., and Ladoux, B. (2015). Adaptive
471 rheology and ordering of cell cytoskeleton govern matrix rigidity sensing. Nat. Commun. 6,
472 7525. doi: 10.1038/ncomms8525.
473 11. Jain, N., Iyer, K.V., Kumar, A., and Shivashankar, G.V. (2013). Cell geometric
474 constraints induce modular gene-expression patterns via redistribution of HDAC3 regulated
475 by actomyosin contractility. Proc. Natl. Acad. Sci. USA 110, 11349-11354. doi:
476 10.1073/pnas.1300801110.
477 12. Denais, C.M., Gilbert, R.M., Isermann, P., McGregor, A.L., te Lindert, M., Weigelin,
478 B., Davidson, P.M., Friedl, P., Wolf, K., and Lammerding, J. (2016). Nuclear envelope
479 rupture and repair during cancer cell migration. Science 352, 353-358. doi:
480 10.1126/science.aad7297.
481 13. Raab, M., Gentili, M., de Belly, H., Thiam, H.R., Vargas, P., Jimenez, A.J.,
482 Lautenschlaeger, F., Voituriez, R., Lennon-Duménil, A.M., Manel, N., et al. (2016). ESCRT
483 III repairs nuclear envelope ruptures during cell migration to limit DNA damage and cell
484 death. Science 352, 359-362. doi: 10.1126/science.aad7611.

485 14. Irianto, J., Xia, Y., Pfeifer, C.R., Athirasala, A., Ji, J., Alvey, C., Tewari, M., Bennett,
486 R.R., Harding, S.M., Liu, A.J., Greenberg, R.A., and Discher, D.E. (2017). DNA damage
487 follows repair factor depletion and portends genome variation in cancer cells after pore
488 migration. Curr. Biol. 27, 210-223. doi: 10.1016/j.cub.2016.11.049.
489 15. Pfeifer, C.R., Xia, Y, Zhu, K., Liu, D., Irianto, J., García, V.M.M., Millán, L.M.S.,
490 Niese, B., Harding, S., Deviri, D., et al. (2019). Constricted migration increases DNA damage
491 and independently represses cell cycle. Mol. Biol. Cell 29, 1948-1962. doi: 10.1091/mbc.E18-
492 02-0079.
493 16. Cho, S., Irianto, J., and Discher, D.E. (2017). Mechanosensing by the nucleus: From
494 pathways to scaling relationships. J. Cell Biol. 216, 305-315. doi: 10.1083/jcb.201610042.
495 17. Ingber, D.E. (2013). Mechanobiology and diseases of mechanotransduction. Ann.
496 Med. 35, 564- 577. doi: 10.1080/07853890310016333.
497 18. Madrazo, E., González-Novo, R., Ortiz-Placín, C., García de Lacoba, M., Gonález-
498 Murillo, Á., Ramírez, M., and Redondo-Muñoz, J. (2022). Fast H3K9 methylation promoted
499 by CXCL12 contributes to nuclear changes and invasiveness of T-acute lymphoblastic
500 leukemia cells. Oncogene 41, 1324-1336. doi: 10.1038/s41388-021-02168-8.
501 19. Harada, T., Swift, J., Irianto, J., Shin, J.W., Spinler, K.R., Athirasala, A., Diegmiller,
502 R., Dingal, P.C., Ivanovska, I.L., and Discher, D.E. (2014). Nuclear lamin stiffness is a barrier
503 to 3D migration, but softness can limit survival. J. Cell Biol. 204, 669-82. doi:
504 10.1083/jcb.201308029.
505 20. Uhler, C., and Shivashankar, G.V. (2017). Regulation of genome organization and
506 gene expression by nuclear mechanotransduction. Nat. Rev. Mol. Cell Biol. 18, 717-727. doi:
507 10.1038/nrm.2017.101.
508 21. Le, H.Q., Ghatak, S., Yeung, C.Y., Tellkamp, F., Günschmann, C., Dieterich, C.,
509 Yeroslaviz, A., Habermann, B., Pombo, A., Niessen, C.M., et al. (2016). Mechanical

510 regulation of transcription controls Polycomb-mediated gene silencing during lineage
511 commitment. Nat. Cell Biol. 218, 864-875. doi: 10.1038/ncb3387.
512 22. Picariello, H.S., Kenchappa, R.S., Rai, V., Crish, J.F., Dovas, A., Pogoda, K.,
513 McMahon, M., Bell, E.S., Chandrasekharan, U., Luu, A., et al. (2019). Myosin IIA suppresses
514 glioblastoma development in a mechanically sensitive manner. Proc. Natl. Acad. Sci. USA
515 116:15550-15559. doi: 10.1073/pnas.1902847116.
516 23. Cho, S., Vashisth, M., Abbas, A., Majkut, S., Vogel, K., Xia, Y., Ivanovska, I.L.,
517 Irianto, J., Tewari, M., Zhu, K., Tichy, E.D., et al. (2019). Mechanosensing by the lamina
518 protects against nuclear rupture, DNA damage, and cell-cycle arrest. Dev. Cell 49, 920-
519 935.e5. doi: 10.1016/j.devcel.2019.04.020.
520 24. Irianto, J., Xia, Y., Pfeifer, C.R., Greenberg, R.A., and Discher, D.E. (2017). As a
521 nucleus enters a small pore, chromatin stretches and maintains integrity, even with DNA
522 breaks. Biophys. J. 112, 446-449. doi: 10.1016/j.bpj.2016.09.047.
523 25. Akman, M., Belisario, D.C., Salaroglio, I.C., Kopecka, J., Donadelli, M., De Smaele,
524 E., and Riganti C. (2021). Hypoxia, endoplasmic reticulum stress and chemoresistance:
525 dangerous liaisons. J. Exp. Clin. Cancer Res. 40, 28. doi: 10.1186/s13046-020-01824-3.
526 26. Toksvang, L.N., Lee, S.H.R., Yang, J.J., and Schmiegelow, K. (2022). Maintenance
527 therapy for acute lymphoblastic leukemia: basic science and clinical translations. Leukemia
528 36, 1749-1758. doi: 10.1038/s41375-022-01591-4.
529 27. Stephens, A.D., Liu, P.Z., Banigan, E.J., Almassalha, L.M., Backman, V., Adam,
530 S.A., Goldman, R.D., and Marko, J.F. (2018). Chromatin histone modifications and rigidity
531 affect nuclear morphology independent of lamins. Mol. Biol. Cell 29, 220-233. doi:
532 10.1091/mbc.E17-06-0410.

533 28. Le Berre, M., Aubertin, J., and Piel, M. (2012). Fine control of nuclear confinement
534 identifies a threshold deformation leading to lamina rupture and induction of specific genes.
535 Integr. Biol. 4, 1406-1414. doi: 10.1039/c2ib20056b.
536 29. Finan, J.D., and Guilak, F. (2010). The effects of osmotic stress on the structure and
537 function of the cell nucleus. J. Cell Biochem. 109, 460-467. doi: 10.1002/jcb.22437.
538 30. Valent, P., Sadovnik, I., Eisenwort, G., Herrmann, H., Bauer, K., Mueller, N., Sperr,
539 W.R., Wicklein, D., and Schumacher U. (2020). Redistribution, homing and organ-invasion
540 of neoplastic stem cells in myeloid neoplasms. Semin. Cancer Biol. 60, 191-201. doi:
541 10.1016/j.semcancer.2019.07.025.
542 31. Croft, D.R., Coleman, M.L., Li, S., Robertson, D., Sullivan, T., Stewart, C.L., and
543 Olson, M.F. (2005). Actin myosin-based contraction is responsible for apoptotic nuclear
544 disintegration. J. Cell Biol. 168, 245-255. doi: 10.1083/jcb.200409049.
545 32. Hatch, M.E., and Hetzer, M.W. (2016). Nuclear envelope rupture is induced by actin-
546 based nucleus confinement. J. Cell Biol. 215, 27-36. doi: 10.1083/jcb.201603053.
547 33. Mall, M., Walter, T., Gorjánácz, M., Davidson, I.F., Nga Ly-Hartig, T.B., Ellenberg,
548 J., and Mattaj, I.W. (2012). Mitotic lamin disassembly is triggered by lipid-mediated
549 signaling. J. Cell Biol. 198, 981-990. doi: 10.1083/jcb.201205103.
550 34. Takaki, T., Montagner, M., Serres, M.P., Le Berre, M., Russell, M., Collinson, L.,
551 Szuhai, K., Howell, M., Boulton, S.J., Sahai, E., and Petronczki, M. (2017). Actomyosin
552 drives cancer cell nuclear dysmorphia and threatens genome stability. Nat Comms.
553 2017;8:16013. doi: 10.1038/ncomms16013.
554 35. Buxboim, A., Swift, J., Irianto, J., Spinler, K.R., Dingal, P.C., Athirasala, A., Kao,
555 Y.R., Cho, S., Harada, T., Shin, J.W., and Discher, D.E. (2014). Matrix elasticity regulates
556 lamin-A,C phosphorylation and turnover with feedback to actomyosin. Curr. Biol. 24, 1909-
557 17. doi: 10.1016/j.cub.2014.07.001.

558 36. Hurst, V., Challa, K., Shimada, K., and Gasser, S.M. (2021). Cytoskeleton integrity
559 influences XRCC1 and PCNA dynamics at DNA damage. Mol. Biol. Cell 32,br6. doi:
560 10.1091/mbc.E20-10-0680.
561 37. Wang, L., Wang, M., Wang, S., Qi, T., Guo, L., Li, J., Qi, W., Ampah, K.K., Ba, X.,
562 and Zeng, X. (2013). Actin polymerization negatively regulates p53 function by impairing its
563 nuclear import in response to DNA damage. PLoS One 8, e60179. doi:
564 10.1371/journal.pone.0060179.
565 38. Dahl, K.N., Ribeiro, A.J.S., and Lammerding, J. (2008). Nuclear shape, mechanics,
566 and mechanotransduction. Circ. Res. 102, 1307-1318. doi:
567 10.1161/CIRCRESAHA.108.173989.
568 39. Zwerger, M., Ho, C.Y., and Lammerding, J. (2011). Nuclear mechanics in disease.
569 Annu. Rev. Biomed. Eng. 13, 397-428. doi: 10.1146/annurev-bioeng-071910-124736.
570 40. Charras, G., and Sahai, E. (2014). Physical influences of the extracellular environment
571 on cell migration. Nat. Rev. Mol. Cell Biol. 15, 813-824. doi: 10.1038/nrm3897.
572 41. Yamada, K.M., Collins, J.W., Cruz Walma, D.A., Doyle, A.D., Morales, S.G., Lu, J.,
573 Matsumoto, K., Nazari, S.S., Sekiguchi, R., Shinsato, Y., and Wang, S. (2019). Extracellular
574 matrix dynamics in cell migration, invasion and tissue morphogenesis. Int. J. Exp. Path. 100,
575 144-152. doi: 10.1111/iep.12329.
576 42. Liu, Y.J., Le Berre, M., Lautenschlaeger, F., Maiuri, P., Callan-Jones, A., Heuzé, M.,
577 Takaki, T., Voituriez, R., and Piel, M. (2015). Confinement and low adhesion induce fast
578 amoeboid migration of slow mesenchymal cells. Cell 160, 659-672. doi:
579 10.1016/j.cell.2015.01.007.
580 43. Yang, C., Del Rio, F.W., Ma, H., Killaars, A.R., Basta, L.P., Kyburz, K.A., and
581 Anseth, K.S. (2016). Spatially patterned matrix elasticity directs stem cell fate. Proc. Natl.
582 Acad. Sci. USA 113, E4439-E4445. doi: 10.1073/pnas.1609731113.

583 44. Heo, S.J., Han, W.M., Szczesny, S.E., Cosgrove, B.D., Elliott, D.M., Lee, D.A.,
584 Duncan, R.L., and Mauck, R.L. (2016). Mechanically induced chromatin condensation
585 requires cellular contractility in mesenchymal stem cells. Biophys. J. 111, 864-874. doi:
586 10.1016/j.bpj.2016.07.006.
587 45. Stefanello, S.T., Luchtefeld, I., Liashkovich, I., Pethö, Z., Azzam, I., Bulk, E., Rosso,
588 G., Döhlinger, L., Hesse, B., Oeckinghaus, A., Shahin, V. (2021). Impact of the Nuclear
589 Envelope on Malignant Transformation, Motility, and Survival of Lung Cancer Cells. Adv
590 Sci (Weinh). 8, e2102757. doi: 10.1002/advs.202102757.
591 46. Xia, Y., Pfeifer, C.R., Zhu, K., Irianto, J., Liu, D., Pannell, K., Chen, E.J., Dooling,
592 L.J., Tobin, M.P., Wang, M,, et al. (2019). Rescue of DNA damage after constricted
593 migration reveals a mechano-regulated threshold for cell cycle. J. Cell Biol. 218, 2545-2563.
594 doi: 10.1083/jcb.201811100.
595 47. Irianto, J., Pfeifer, C.R., Bennett, R.R., Xia, Y., Ivanovska, I.L., Liu, A.J., Greenberg,
596 R.A., and Discher, D.E. (2017). Nuclear constriction segregates mobile nuclear proteins away
597 from chromatin. Mol. Biol. Cell 27, 4011-4020. doi: 10.1091/mbc.E16-06-0428.
598 48. Shah, P., Hobson, C.M., Cheng, S., Colville, M.J., Paszek, M.J., Superfine, R., and
599 Lammerding, J. (2021). Nuclear deformation causes DNA damage by increasing replication
600 stress. Curr. Biol. 31, 1-13. doi: 10.1016/j.cub.2020.11.037.
601 49. Engler, A.J., Sen, S., Sweeney, H.L., and Discher, D.E. (2006). Matrix elasticity
602 directs stem cell lineage specification. Cell 126, 677-689. doi: 10.1016/j.cell.2006.06.044.
603 50. Killaars, A.R., Grim, J.C., Walker, C.J., Hushka, E.A., Brown, T.E., and Anseth, K.S.
604 (2018). Extended exposure to stiff microenvironments leads to persistent chromatin
605 remodeling in human mesenchymal stem cells. Adv. Sci. (Weinh) 6, 1801483. doi:
606 10.1002/advs.201801483.

607 51. Downing, T.L., Soto, J., Morez, C., Houssin, T., Fritz, A., Yuan, F., Chu, J., Patel, S.,
608 Schaffer, D.V., and Li, S. (2013). Biophysical regulation of epigenetic state and cell
609 reprogramming. Nat. Mater. 12, 1154-1162. doi: 10.1038/nmat3777.
610 52. Werner, M., Blanquer, S.B., Haimi, S.P., Korus, G., Dunlop, J.W., Duda, G.N.,
611 Grijpma, D.W., Petersen, A. (2016). Surface Curvature Differentially Regulates Stem Cell
612 Migration and Differentiation via Altered Attachment Morphology and Nuclear Deformation.
613 Adv Sci (Weinh). 4, 1600347. doi: 10.1002/advs.201600347.
614 53. Uroz, M., Wistorf, S., Serra-Picamal, X., Conte, V., Sales-Pardo, M., Roca-Cusachs,
615 P., and Trepat, X. (2018). Regulation of cell cycle progression by cell-cell and cell-matrix
616 forces. Nat. Cell Biol. 20, 461-654. doi: 10.1038/s41556-018-0107-2.
617 54. Gemble, S., Wardenaar, R., Keuper, K., Srivastava, N., Nano, M., Macé, A.S., Tijhuis,
618 A.E., Bernhard, S.V., Spierings, D.C.J., Simon, A., et al. Genetic instability from a single S
619 phase after whole-genome duplication. Nature. 2018, 604:146-151. doi: 10.1038/s41586-022-
620 04578-4.
621 55. Guilluy, C., Osborne, L.D., Van Landeghem, L., Sharek, L., Superfine, R., Garcia-
622 Mata, R., and Burridge, K. (2014). Isolated nuclei adapt to force and reveal a
623 mechanotransduction pathway in the nucleus. Nat. Cell Biol. 16, 376-381. doi:
624 10.1038/ncb2927.
625 56. Furusawa, T., Rochman, M., Taher, L., Dimitriadis, E.K., Nagashima, K., Anderson,
626 S., and Bustin, M. (2015). Chromatin decompaction by the nucleosomal binding protein
627 HMGN5 impairs nuclear sturdiness. Nat. Commun. 6, 6138. doi: 10.1038/ncomms7138.
628 57. Zhang, X., Cook, P.C., Zindy, E., Williams, C.J., Jowitt, T.A., Streuli, C.H.,
629 MacDonald, A.S., and Redondo-Muñoz, J. (2016). et al. Integrin α4β1 controls G9a activity
630 that regulates epigenetic changes and nuclear properties required for lymphocyte migration.
631 Nucleic Acids Res. 44, 3031-44. doi: 10.1093/nar/gkv1348.

632 58. Wang, P., Dreger, M., Madrazo, E., Williams, C.J., Samaniego, R., Hodson, N.W.,
633 Monroy, F., Baena, E., Sánchez-Mateos, P., Hurlstone, A., et al. (2020). WDR5 modulates
634 cell motility and morphology and controls nuclear changes induced by a 3D environment.
635 Proc Natl Acad Sci USA. 2020;115:8581-8586. doi: 10.1073/pnas.1719405115.
636 59. Kumar, A., Mazzanti, M., Mistrik, M., Kosar, M., Beznoussenko, G.V., Mironov,
637 A.A., Garrè, M., Parazzoli, D., Shivashankar, G.V., Scita, G., et al. (2014). ATR mediates a
638 checkpoint at the nuclear envelope in response to mechanical stress. Cell 158, 633-646. doi:
639 10.1016/j.cell.2014.05.046.
640 60. Aureille, J., Buffiere-Ribot, V., Harvey, B.E., Boyault, C., Pernet, L., Andersen, T.,
641 Bacola, G., Balland, M., Fraboulet, S., Van Landeghem, L., and Guilluy, C. (2019). Nuclear
642 envelope deformation controls cell cycle progression in response to mechanical force. Embo
643 Rep. 20, e48084. doi: 10.15252/embr.201948084.
644 61. Karran, P., and Attard, N. (2008). Thiopurines in current medical practice: molecular
645 mechanisms and contributions to therapy-related cancer. Nat. Rev. Cancer. 8, 24-36. doi:
646 10.1038/nrc2292.
647 62. Oakes, S.A. (2020). Endoplasmic reticulum stress signaling in cancer cells. Am. J.
648 Pathol. 190, 934-946. doi: 10.1016/j.ajpath.2020.01.010.
649 63. Meador, J.A., Zhao, M., Su, Y., Narayan, G., Geard, C.R., and Balajee, A.S. (2008).
650 Histone H2AX is a critical factor for cellular protection against DNA alkylating agents.
651 Oncogene 27, 5662-5671. doi: 10.1038/onc.2008.187.
652 64. Celeste, A., Petersen, S., Romanienko, P.J., Fernandez-Capetillo, O., Chen, H.T.,
653 Sedelnikova, O.A., Reina-San-Martin, B., Coppola, V., Meffre, E., Difilippantonio, M.J., et
654 al. (2002). Genomic instability in mice lacking histone H2AX. Science 296, 922-927. doi:
655 10.1126/science.1069398.

656 65. Tusamda Wakhloo, N., Anders, S., Badique, F., Eichhorn, M., Brigaud, I., Petithory,
657 T., Vassaux, M., Milan, J.L., Freund, J.N., Rühe, J., et al., (2020). Actomyosin, vimentin and
658 LINC complex pull on osteosarcoma nuclei to deform on micropillar topography.
659 Biomaterials 234, 119746. doi: 10.1016/j.biomaterials.2019.119746. E
660 66. Schrank, B.R., Aparicio, T., Li, Y., Chang, W., Chait, B.T., Gundersen, G.G.,
661 Gottesman, M.E., and Gautier, J. (2018). Nuclear Arp2/3 drives DNA break clustering for
662 homology-directed repair. Nature 559, 61-66. doi: 10.1038/s41586-018-0237-5
663 67. Mistriotis, P., Wisniewski, E.O., Bera, K., Keys, J., Li, Y., Tuntithavornwat, S., Law,
664 R.A., Perez-Gonzalez, N.A., Erdogmus, E., Zhang, Y., Zhao, R., et al. (2019). Confinement
665 hinders motility by inducing RhoA-mediated nuclear influx, volume expansion and blebbing.
666 J. Cell Biol. 218, 4093-4111. doi: 10.1083/jcb.201902057.
667 68. Makhija, E., Jokhun, D.S., and Shivashankar, G.V. (2016). Nuclear deformability and
668 telomere dynamics are regulated by cell geometric constraints. Proc. Natl. Acad. Sci. USA
669 113, E32-E40. doi: 10.1073/pnas.1513189113.
670 69. Patteson, A.E., Vahabikashi, A., Pogoda, K., Adam, S.A., Mandal, K., Kittisopikul,
671 M., Sivagurunathan, S., Goldman, A., Goldman, R.D., and Janmey, P.A. (2019). Vimentin
672 protects cells against nuclear rupture and DNA damage during migration. J. Cell Biol. 218,
673 4079-4092. doi: 10.1083/jcb.201902046.
674

674 **Figure Legends**

675 **Figure 1: Cell migration through constrictions governs nuclear changes in leukemia**
676 **cells. (A)** Jurkat cells were allowed to migrate across 3 μm transwell inserts for 24h. Non-
677 migrating and one-round migrated (ORM) cells were collected from the upper and bottom
678 chambers, respectively, sedimented on poly-L-lysine coated coverslips, fixed and stained with
679 DAPI (blue) for their analysis by confocal microscopy. Right panels indicate in black the area
680 of the nuclei. Bar 10 μm. **(B)** Graph shows changes in the nuclear area of Jurkat cells upon
681 one-round of migration through constrictions. Mean n= 157 cells ± SD (3 replicates). **(C)**
682 Jurkat and CCRF-CEM cells were forced to migrate several rounds through 3 μm transwell
683 inserts. Then, migrated cells were collected as migratory-altered (MA) cells, expanded and
684 kept in culture conditions. **(D)** Control and MA Jurkat cells were sedimented on poly-L-lysine
685 coated coverslips, fixed and stained with DAPI. Right panels indicate in black the area of the
686 nuclei. Bar 10 μm. **(E)** Graph shows changes in the nuclear area of control and MA cells.
687 Mean n= 216 cells ± SD (5 replicates). **(F)** Control and MA Jurkat cells were collected and
688 processed for thin section electron microscopy to visualize the nuclear morphology. Plot
689 shows changes in the nuclear circularity of control and MA Jurkat cells (n=6 representative
690 cells).

691 **Figure 2: Confined migration alters the lamin B1 distribution of moving cells.** (A) Non-
692 migrating and ORM Jurkat cells were seeded on poly-L-lysine-coated glasses and stained
693 with DAPI (blue) and anti-lamin B1 antibody (red) for their analysis by confocal microscopy.
694 Bar 10 μm. (B) Line plots show the signal profile of lamin B1 from 15 representative nuclei.
695 Red line indicates the mean intensity of the profiles analyzed. (C) Control, fresh ORM, and
696 ORM Jurkat cells collected and cultured in suspension for an additional 24 h were seeded on
697 poly-L-lysine-coated glasses and analyzed by confocal microscopy. Bar 10 μm. (D) Graph
698 shows changes in the nuclear area of the cells from (C). Mean n=25-92 cells ± SD (2

699 independent replicates). (E) Line plots show the signal profile of lamin B1 from 15
700 representative nuclei of the cells from (C). (F) Control and MA Jurkat cells were seeded on
701 poly-L-lysine-coated glasses and analyzed by confocal microscopy. Bar 10 μm. (G) Line
702 plots show the signal profile of lamin B1 from 15 representative nuclei of control and MA
703 Jurkat cells. The red line indicates the mean intensity of the profiles analyzed.

704 **Figure 3: Persistent migration induces enduring changes in the transcriptional profile of**
705 **migrating cells. (A)** Control and MA Jurkat cells were lysed, and transcriptional changes
706 determined by mRNA expression microarray. Heat map shows the relative gene expression
707 patterns of control and MA cells. **(B)** Pathway enrichment analysis based on differentially
708 upregulated genes in MA Jurkat cells. **(C)** Validation of microarray data by protein expression
709 levels. Plot shows the transcript-protein level pairs from 5 randomly selected proteins from
710 the transcriptional analysis by microarray. Gene names, Pearson correlation analysis (r) and P
711 value are indicated. **(D)** Control and MA Jurkat cells were incubated with BrdU for 4 and 18
712 h. Then, cells were fixed and BrdU incorporation quantified. Mean n = 6 replicates ± SD. **(E)**
713 Control (dark line) and MA (dashed line) Jurkat cells were cultured at indicated times and cell
714 proliferation was quantified by MTT assay. Mean n = 3 replicates ± SD. **(F)** Control (in red)
715 and MA (in blue) Jurkat cells were fixed, permeabilized and stained with propidium iodide.
716 Then, cell cycle progression was analyzed by flow cytometry. Graph shows the G1, S and
717 G2/M phases according to DNA content.

718 **Figure 4: Persistent cell migration leads to aberrant DNA damage response. (A)** Non-
719 migrating and ORM Jurkat cells were seeded on poly-L-lysine-coated glasses and stained
720 with DAPI (blue) and anti-γH2AX antibody (red) for their analysis by confocal microscopy.
721 Bar 10 μm. Graph shows the percentage of cells with more than 2 visible foci for γH2AX
722 (dark grey, as high γH2AX signal). Mean n = 116-118 ± SD (3 replicates). **(B)** Control and
723 MA Jurkat cells were seeded on poly-L-lysine-coated glasses, stained, and analyzed by

724 confocal microscopy. Bar 10 μm. Graph shows the percentage of control and MA Jurkat cells
725 with more than 2 visible foci for γH2AX. Mean n = 28-35 cells ± SD (2 replicates). **(C)**
726 Control and MA CCRF-CEM cells were seeded on poly-L-lysine-coated glasses glasses,
727 stained, and analyzed by confocal microscopy. Bar 10 μm. Graph shows the percentage of
728 control and MA CCRF-CEM cells with more than 2 visible foci for γH2AX. Mean n = 146-
729 171 cells ± SD (3 replicates). **(D)** Pathway enrichment analysis based on differentially
730 downregulated genes in MA Jurkat cells. **(E)** Control and MA Jurkat cells were cultured in
731 the presence or not of methotrexate (1 μM) for 24 h. Then, cells were collected and stained
732 with annexin V-FITC and propidium iodide for their flow cytometry analysis. **(F)** Graph
733 shows the survival ratio of control and MA Jurkat cells upon normalization to their untreated
734 conditions. Mean n = 3 ± SD.

735 **Figure 5: Migrated altered cells show altered mechanical and functional properties. (A)**
736 Isolated nuclei from control and MA Jurkat cells were stained with DAPI and seeded on poly-
737 L-lysine-coated coverslips. Confocal sections of the nuclei were taken before (Preconf.) and
738 after (Postconf.) confinement. Bar 10 μm. **(B)** Graph shows the nuclear area from cells in (A).
739 Mean n = 66-89 isolated nuclei ± SD (3 replicates). **(C and D)** Variation of the stiffness (E)
740 and the poroelastic diffusivity coefficient (D) in function of the nuclear indentation depth
741 (shown in terms of strain, ε), both expressed as logarithmic values. Equivalent indentation
742 depth in terms of distance, δ, is shown on top. Black and red dots represent values calculated
743 from experimental data for control (n=124; indentation sites=13; nuclei=6) and MA Jurkat
744 cells (n=115; indentation sites=12; nuclei=5), respectively. Linear fits are included as dashed
745 lines. **(E)** Isolated nuclei from control and MA Jurkat cells were seeded on poly-lysine coated
746 glasses. Then, osmotic stress conditions were induced by the addition of EDTA (swelling
747 conditions) or $MgCl_2$ (shrinking conditions). Nuclei were fixed, permeabilized and stained
748 with DAPI for their analysis by confocal microscopy. Bar 10 μm. **(F)** Graph shows the

749 nuclear area quantified from (C). Mean n = 29-46 isolated nuclei ± SD (2 replicates). **(G)**
750 Control and MA Jurkat cells were seeded on the top of a collagen matrix and allowed to
751 penetrate into the collagen in response to serum (FBS, fetal bovine serum) for 24h. Cells were
752 fixed, stained with propidium iodide and serial confocal sections were captured. Images show
753 the cell penetrability into the collagen. **(H)** Control (Cell Tracker Far Red+) and MA (CFSE+)
754 Jurkat cells were mixed and injected into the tail vein of 10 NSG mice. After 24 h, labeled
755 cells in spleen, liver and bone marrow were determined by flow cytometry. Graph shows the
756 percentage of control and the MA cells analyzed in each animal. Mean n = 10.

757 **Figure 6: Actin polymerization balance regulates the nuclear changes described for MA**
758 **cells. (A)** MA Jurkat cells were cultured in the presence or absence of latrunculin B (1
759 μg/mL) and jasplakinolide (1 μg/mL) for 1h at 37ºC. Then, cells were seeded on poly-L-
760 lysine coated coverslips, fixed and analyzed by confocal microscopy. Bar 10 μm. **(B)** Line
761 plots show the signal profile of lamin B1 from 15 representative nuclei. The red line indicates
762 the mean intensity of the profiles analyzed. **(C)** Graph shows changes in the nuclear area of
763 MA Jurkat cells under indicated treatments. Mean n= 145-185 nuclei ± SD (3 replicates). **(D)**
764 Control and MA Jurkat cells were treated or not with latrunculin B or jasplakinolide for 1h.
765 Then, cells were collected, and their DNA was digested with DNAse for 15 min and resolved
766 in an agarose gel. **(E)** Graph shows the nucleosomal releasing profile from control (dashed
767 line) and MA Jurkat cells as in (D). Arrows indicate the maxima DNA peaks in each cell
768 population. **(F)** Control and MA Jurkat cells were treated or not with latrunculin B or
769 jasplakinolide for 1h. Cells were fixed, permeabilized and stained with DAPI (blue) and
770 γH2AX (red) for their analysis by confocal microscopy. Bar 10 μm. **(G)** Graph shows the
771 percentage of cells with more than 2 visible foci for γH2AX from (F). Mean n= 53-82 nuclei
772 ± SD (3 replicates).
773

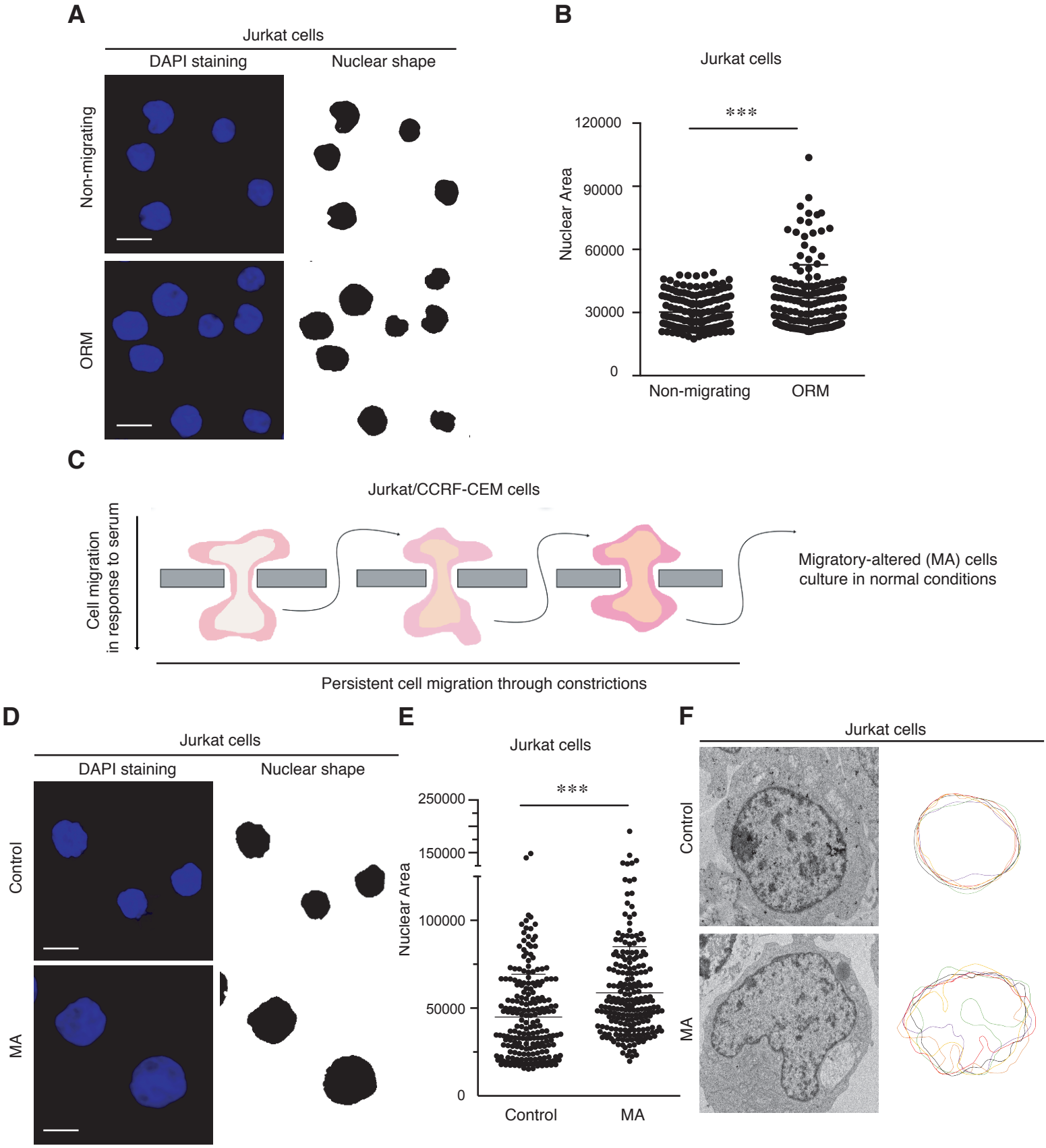
A
Jurkat cells
DAPI staining
Nuclear shape
Non-migrating
ORM
B
Jurkat cells
***
120000
90000
60000
30000
0
Nuclear Area
Non-migrating
ORM
C
Jurkat/CCRF-CEM cells
Cell migration
in response to serum
Migratory-altered (MA) cells
culture in normal conditions
Persistent cell migration through constrictions
D
Jurkat cells
DAPI staining
Nuclear shape
Control
MA
E
Jurkat cells
***
250000
150000
100000
50000
0
Nuclear Area
Control
MA
F
Jurkat cells
Control
MA

Figure 1

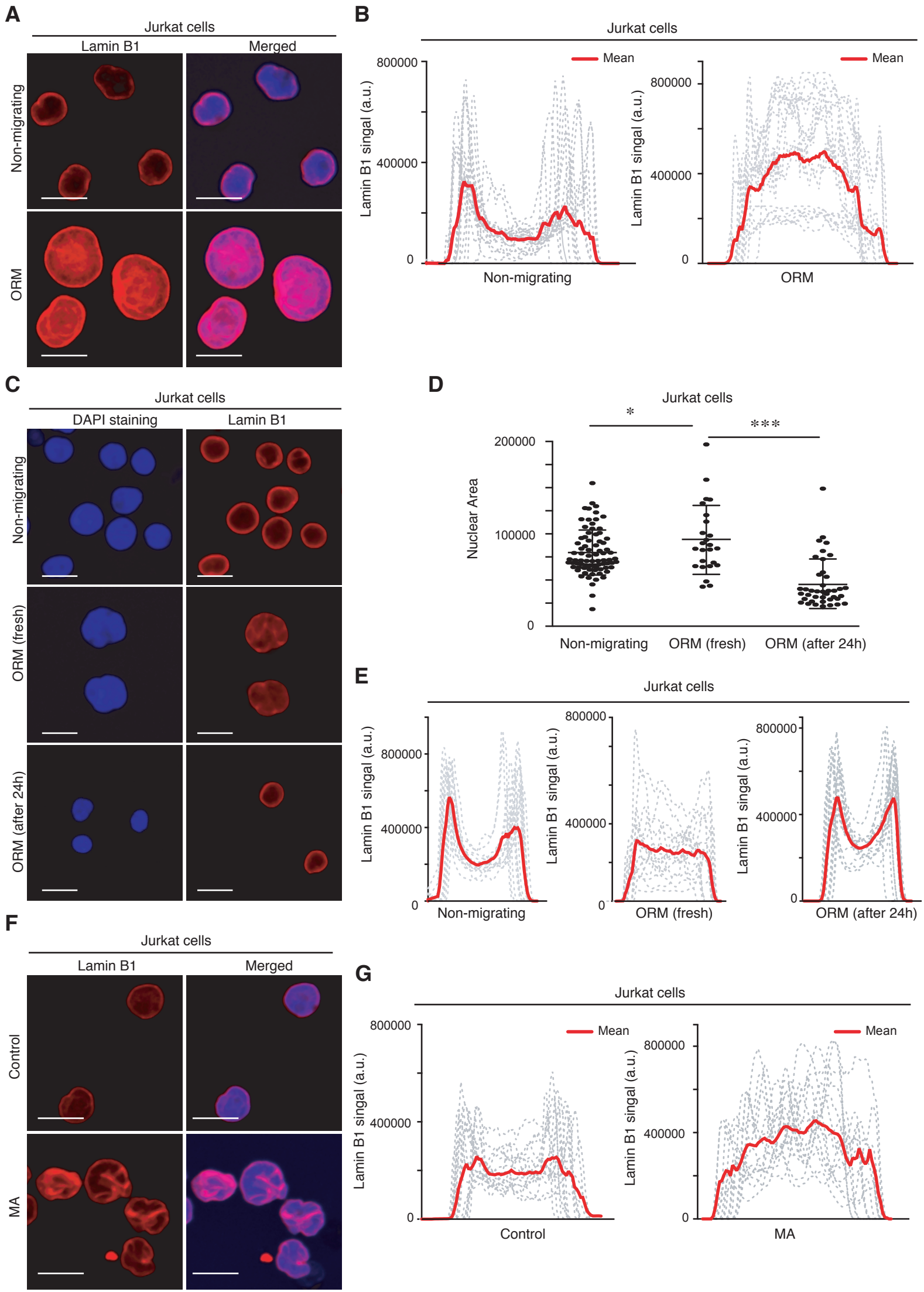
A
Jurkat cells
Lamin B1
Merged
Non-migrating
ORM
B
Jurkat cells
Mean
Lamin B1 singal (a.u.)
800000
400000
0
Non-migrating
ORM
C
Jurkat cells
DAPI staining
Lamin B1
Non-migrating
ORM (fresh)
ORM (after 24h)
D
Jurkat cells
*
***
Nuclear Area
200000
100000
0
Non-migrating
ORM (fresh)
ORM (after 24h)
E
Jurkat cells
Lamin B1 singal (a.u.)
800000
400000
0
Non-migrating
ORM (fresh)
ORM (after 24h)
F
Jurkat cells
Lamin B1
Merged
Control
MA
G
Jurkat cells
Mean
Lamin B1 singal (a.u.)
800000
400000
0
Control
MA

Figure 2

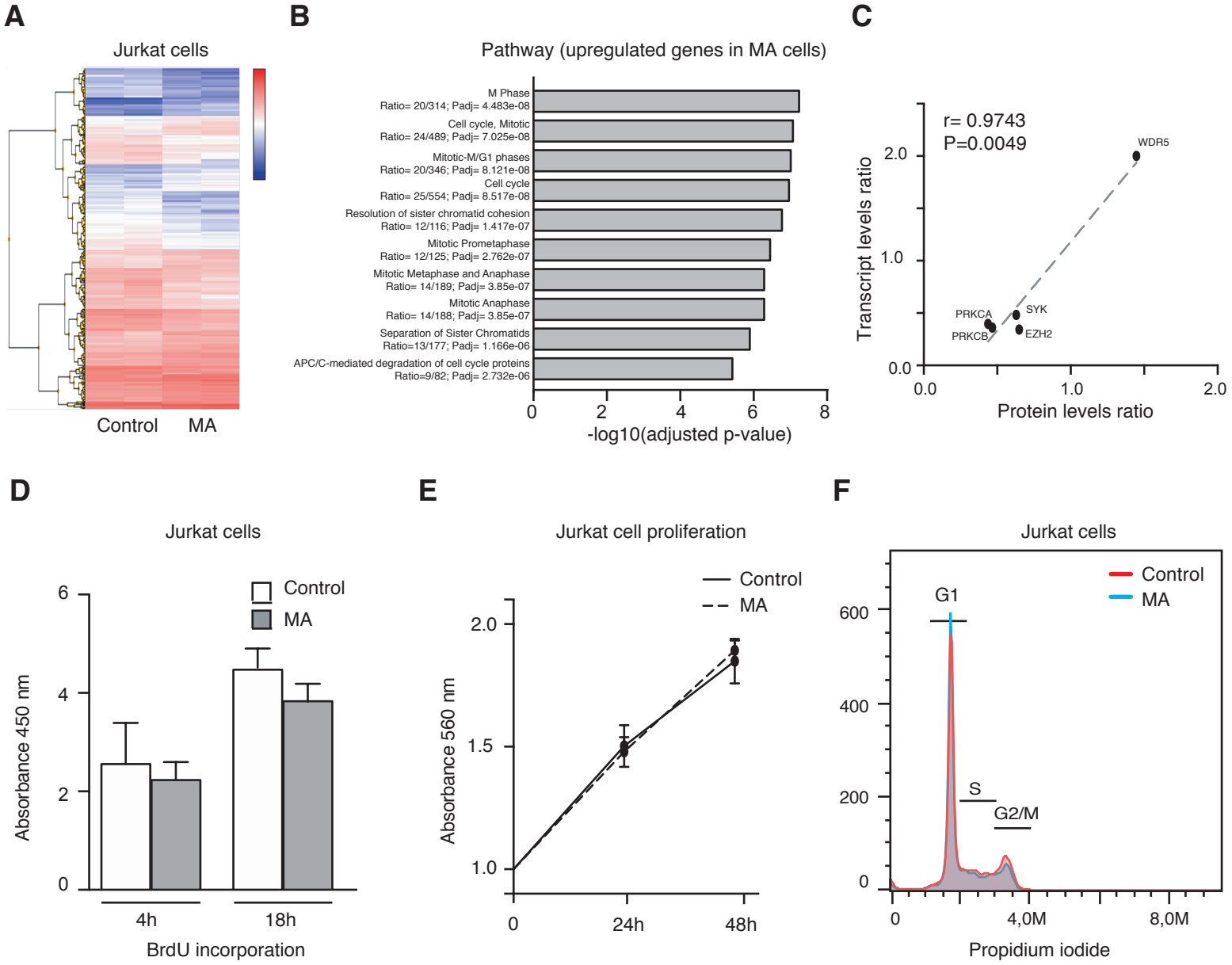
A
Jurkat cells
Control
MA
B
Pathway (upregulated genes in MA cells)
M Phase
Ratio= 20/314; Padj= 4.483e-08
Cell cycle, Mitotic
Ratio= 24/489; Padj= 7.025e-08
Mitotic-M/G1 phases
Ratio= 20/346; Padj= 8.121e-08
Cell cycle
Ratio= 25/554; Padj= 8.517e-08
Resolution of sister chromatid cohesion
Ratio= 12/116; Padj= 1.417e-07
Mitotic Prometaphase
Ratio= 12/125; Padj= 2.762e-07
Mitotic Metaphase and Anaphase
Ratio= 14/189; Padj= 3.85e-07
Mitotic Anaphase
Ratio= 14/188; Padj= 3.85e-07
Separation of Sister Chromatids
Ratio=13/177; Padj= 1.166e-06
APC/C-mediated degradation of cell cycle proteins
Ratio=9/82; Padj= 2.732e-06
0
2
4
6
8
-log10(adjusted p-value)
C
r= 0.9743
P=0.0049
WDR5
SYK
EZH2
PRKCA
PRKCB
Transcript levels ratio
Protein levels ratio
0.0
1.0
2.0
D
Jurkat cells
Control
MA
Absorbance 450 nm
0
2
4
6
4h
18h
BrdU incorporation
E
Jurkat cell proliferation
Control
MA
Absorbance 560 nm
1.0
1.5
2.0
0
24h
48h
F
Jurkat cells
Control
MA
G1
S
G2/M
0
200
400
600
0
4,0M
8,0M
Propidium iodide

Figure 3

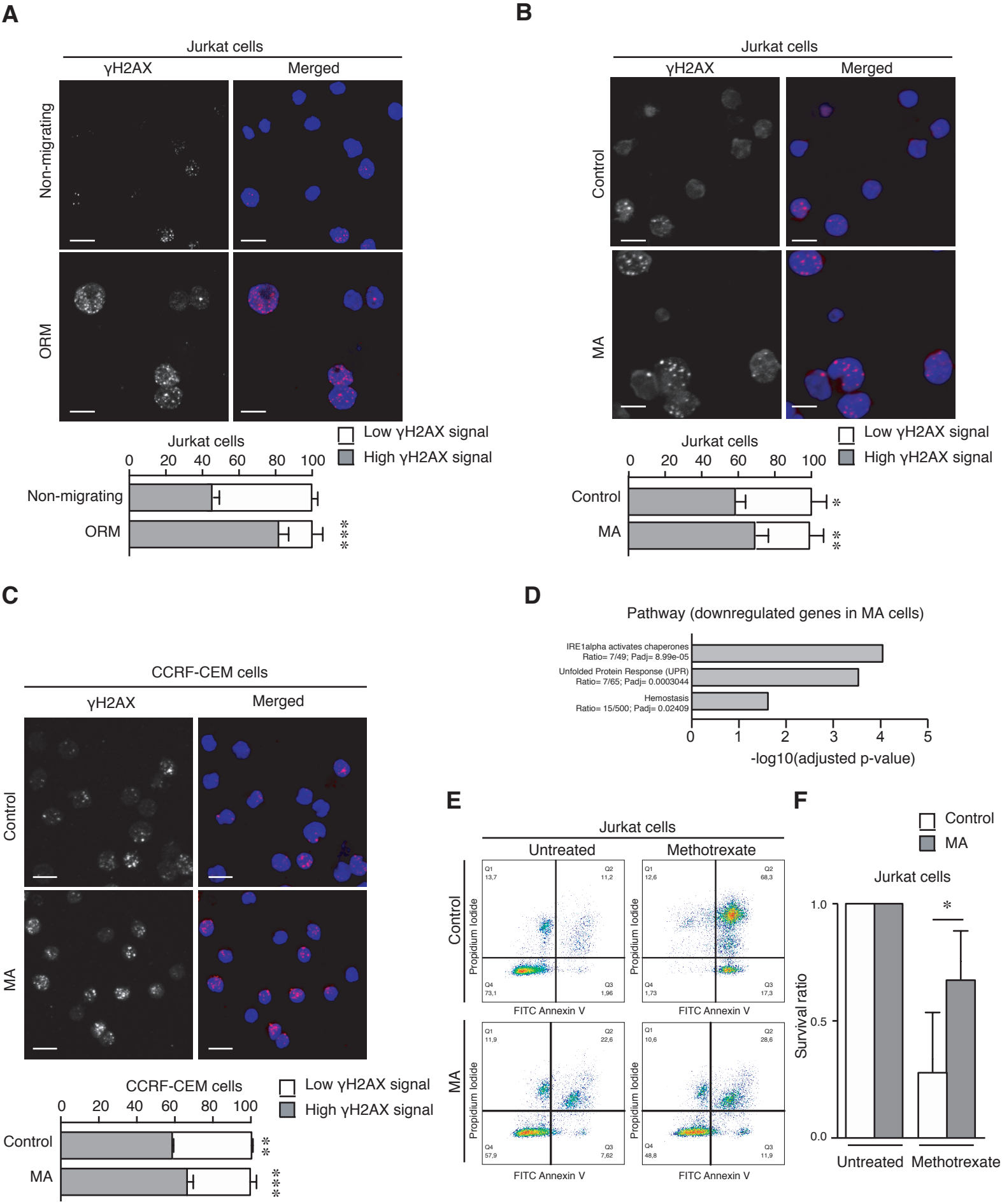
A
Jurkat cells
γH2AX
Merged
Non-migrating
ORM
Jurkat cells
0 20 40 60 80 100
Non-migrating
ORM
Low γH2AX signal
High γH2AX signal
B
Jurkat cells
γH2AX
Merged
Control
MA
Jurkat cells
0 20 40 60 80 100
Control
MA
Low γH2AX signal
High γH2AX signal
C
CCRF-CEM cells
γH2AX
Merged
Control
MA
CCRF-CEM cells
0 20 40 60 80 100
Control
MA
Low γH2AX signal
High γH2AX signal
D
Pathway (downregulated genes in MA cells)
IRE1alpha activates chaperones
Ratio= 7/49; Padj= 8.99e-05
Unfolded Protein Response (UPR)
Ratio= 7/65; Padj= 0.0003044
Hemostasis
Ratio= 15/500; Padj= 0.02409
0 1 2 3 4 5
-log10(adjusted p-value)
E
Jurkat cells
Untreated
Methotrexate
Control
MA
Propidium Iodide
FITC Annexin V
Q1 13,7
Q2 11,2
Q4 73,1
Q3 1,96
Q1 12,6
Q2 68,3
Q4 1,73
Q3 17,3
Q1 11,9
Q2 22,6
Q4 57,9
Q3 7,62
Q1 10,6
Q2 28,6
Q4 48,8
Q3 11,9
F
Control
MA
Jurkat cells
Survival ratio
1.0
0.5
0.0
Untreated
Methotrexate

Figure 4

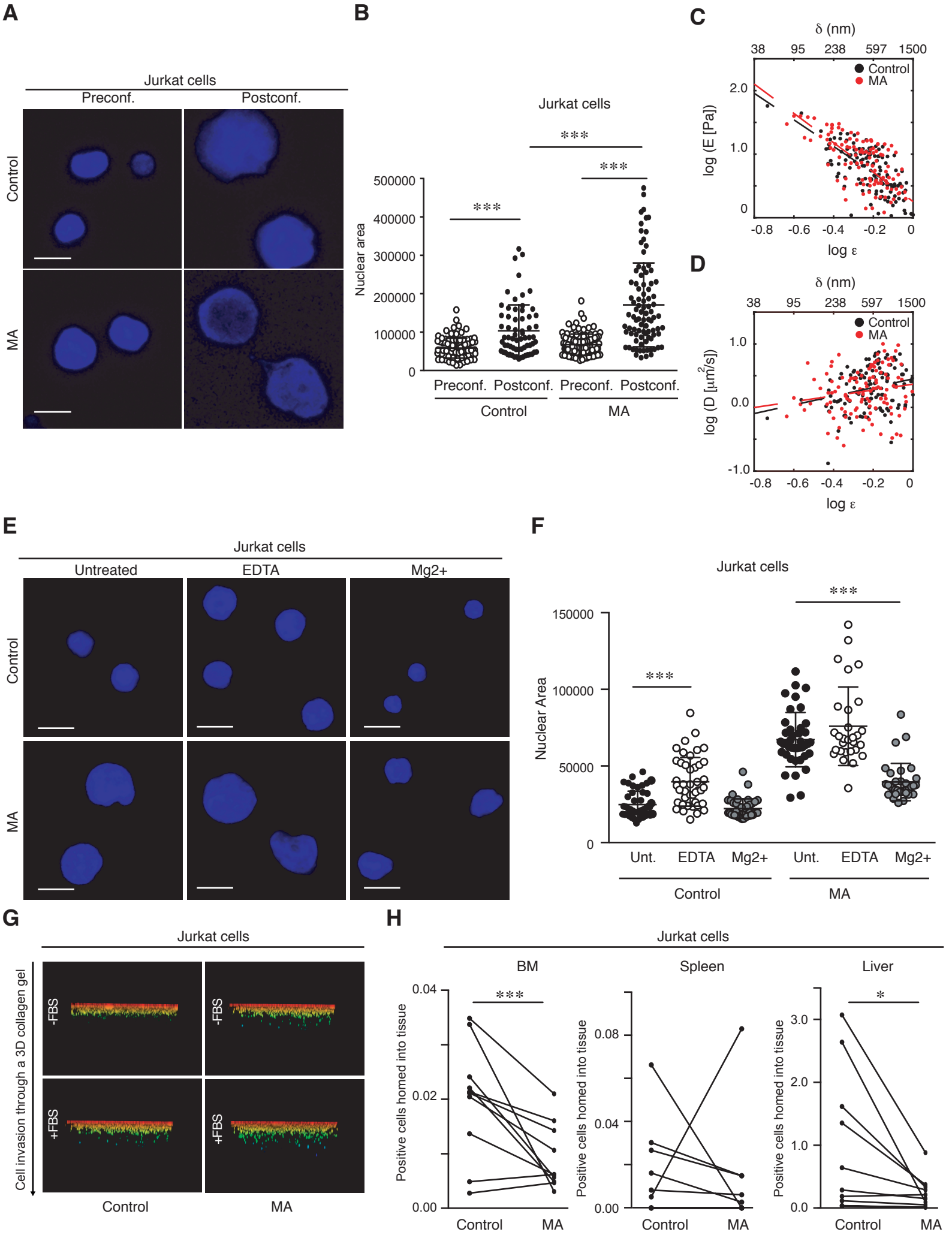
A
Jurkat cells
Preconf.
Postconf.
Control
MA
B
Jurkat cells
***
***
***
Nuclear area
500000
400000
300000
200000
100000
0
Preconf.
Postconf.
Preconf.
Postconf.
Control
MA
C
δ (nm)
38
95
238
597
1500
Control
MA
log (E [Pa])
2.0
1.0
0
-0.8
-0.6
-0.4
-0.2
0
log ε
D
δ (nm)
38
95
238
597
1500
Control
MA
log (D [μm²/s])
1.0
0.0
-1.0
-0.8
-0.6
-0.4
-0.2
0
log ε
E
Jurkat cells
Untreated
EDTA
Mg2+
Control
MA
F
Jurkat cells
***
***
Nuclear Area
150000
100000
50000
0
Unt.
EDTA
Mg2+
Unt.
EDTA
Mg2+
Control
MA
G
Jurkat cells
Cell invasion through a 3D collagen gel
-FBS
-FBS
+FBS
+FBS
Control
MA
H
Jurkat cells
BM
Spleen
Liver
***
*
Positive cells homed into tissue
0.04
0.02
0.00
0.08
0.04
0.00
3.0
2.0
1.0
0.0
Control
MA
Control
MA
Control
MA

Figure 5

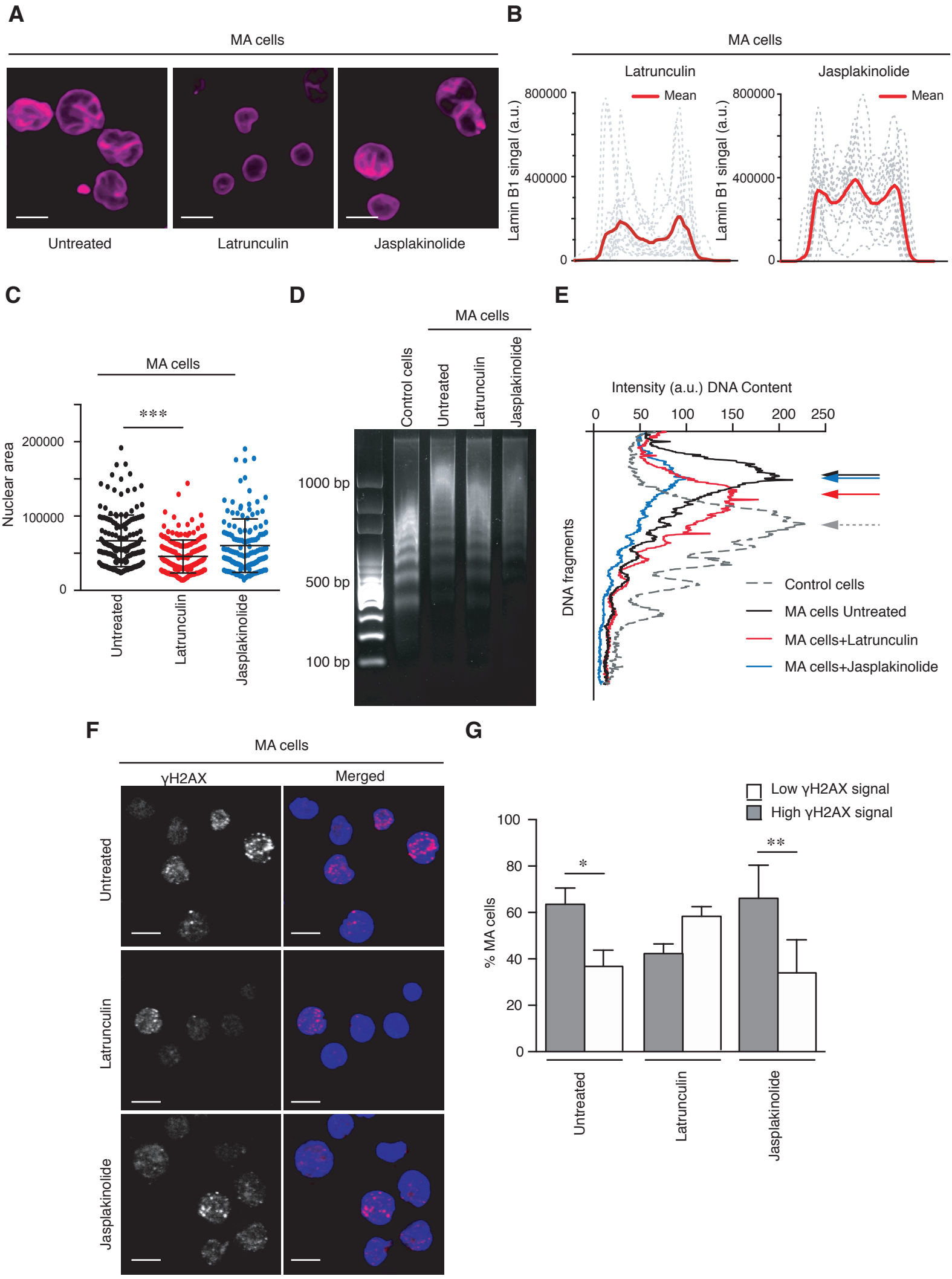
A
MA cells
Untreated
Latrunculin
Jasplakinolide
B
MA cells
Latrunculin
Jasplakinolide
Mean
Lamin B1 singal (a.u.)
800000
400000
0
C
MA cells
***
Nuclear area
200000
100000
0
Untreated
Latrunculin
Jasplakinolide
D
MA cells
Control cells
Untreated
Latrunculin
Jasplakinolide
1000 bp
500 bp
100 bp
E
Intensity (a.u.) DNA Content
0
50
100
150
200
250
DNA fragments
Control cells
MA cells Untreated
MA cells+Latrunculin
MA cells+Jasplakinolide
F
MA cells
γH2AX
Merged
Untreated
Latrunculin
Jasplakinolide
G
Low γH2AX signal
High γH2AX signal
% MA cells
100
80
60
40
20
0
*
**
Untreated
Latrunculin
Jasplakinolide

Figure 6